LAD-Enhancer: A Lightweight All in One Aerial Detection Enhancer Under Adverse Weather

Yu Wan[1], Li Jie[1], Lin Liupeng[2], Zhang Zaiyan[1], Yuan Qiangqiang[1], Shen Huanfeng[2]

1.School of Geodesy and Geomatics, Wuhan University, Wuhan 430079, China
2.School of Resource and Environmental Sciences, Wuhan University, Wuhan 430079, China
*Corresponding author, E-mail address: jli89@sgg.whu.edu.cn

Keywords: Object Detection, Aerial Images, Lightweight, All in One Model, Mixture of Experts.

Abstract

With the rapid development of aerial imaging technology, aerial target detection has become a research hotspot with broad applications in intelligent transportation, agricultural monitoring, and military surveillance. However, the performance of aerial detection models is often degraded under adverse weather conditions such as fog, sandstorms, and low illumination. In such environments, aerial images typically suffer from reduced contrast and color distortion, which significantly affects the model’s ability to accurately identify targets. To this end, a Lightweight All-in-One Aerial Detection Enhancer Under Adverse Weather (LAD-Enhancer) has been proposed. The designed enhancer processes and restores degraded aerial images, thereby enhancing the detection model’s ability to perceive potential targets. Unlike conventional image restoration models, LAD-Enhancer integrates detection labels as additional supervision during training to ensure that enhancement is detection-oriented rather than purely visual. Furthermore, a three-stage training strategy and a Mixture of Experts (MoE) framework are employed to adaptively classify and process images captured under different degradation conditions. Experimental results demonstrate that, with an increase of fewer than 3K parameters, the proposed model significantly improves detection performance under adverse weather conditions while maintaining almost unchanged performance on clear-weather images.

1. Introduction

The aerial object detection plays a crucial role in various applications, including intelligent transportation (Yang et al., 2023; Zhang et al., 2014), agricultural monitoring (Badgujar et al., 2024), and disaster detection (Zhao et al., 2024). However, due to its unique aerial perspective, aerial detection is highly vulnerable to adverse weather conditions. Under such degraded environments, aerial images often suffer from reduced contrast and color distortion, which significantly impairs the accuracy of detection models in identifying targets. To address this issue, existing studies have primarily adopted three strategies: direct methods, distributed methods, and union methods (Wan et al., 2025). Direct methods train detection models directly on degraded images, enabling the model to adapt to challenging weather conditions (Wang et al., 2021; Xia et al., 2022). Distributed methods (Li and Zhao, 2023; Liu et al., 2019; Long et al., 2014; Qin et al., 2020; Qiu et al., 2023; Zhang et al., 2025; Zhang et al., 2020) employ image restoration techniques as a preprocessing step before detection to recover clearer visual features. Union methods (Huang et al., 2021) jointly optimize image restoration and detection networks, maintaining consistency between feature restoration and target detection while effectively handling complex degraded scenarios. However, both direct and union methods, though effective in enhancing detection performance under adverse conditions, require retraining of detection models, which is often impractical in real-world industrial applications. In contrast, distributed methods primarily emphasize visual restoration quality, while often neglecting their actual impact on detection performance.

To this end, we propose a Lightweight All-in-One Aerial Detection Enhancer under Adverse Weather (LAD-Enhancer) to achieve plug-and-play adaptability and effectively support aerial detection tasks. The LAD-Enhancer can be seamlessly integrated before existing detection models without retraining or parameter adjustment, significantly improving detection performance under adverse weather conditions. Meanwhile, with fewer than 3K parameters, the enhancer meets the demand for lightweight requirements in aerial detection.

To address the three primary degradation scenarios in aerial target detection, including foggy, dusty, and low-light conditions, a Mixture of Experts (MoE) architecture is incorporated, enabling adaptive processing tailored to each scenario. Moreover, since conventional image restoration models may inadvertently degrade the quality of already clear images, thereby diminishing detection accuracy, an initial classifier is introduced in the first stage to distinguish between clear and degraded images. This effectively reduces over-enhancement and preserves the integrity of clear inputs. Furthermore, to mitigate contrast reduction and color distortion commonly observed under adverse weather conditions, a multi-space restoration loss and an enhance module with detection enhancement loss are proposed. The multi-space restoration loss constrains color recovery of the MoE module across multiple color spaces, correcting color distortions, while the enhancement module after the MoE module leverages detection labels to guide the network toward salient target regions, improving both contrast and target visibility.

In summary, the key contributions of this work are as follows:

(1) A plug-and-play Lightweight All-in-One Aerial Detection Enhancer is proposed to improve the detection performance under adverse weather conditions.

(2) The integration of an initial classifier and a Mixture of Experts (MoE) framework enables adaptive enhancement across multiple degradation scenarios while minimizing interference with clear images.

(3) A Multi-Space Restoration Loss and an Enhance Module with Detection Enhancement Loss are designed to address color distortion and target contrast reduction under adverse weather.

This contribution has been peer-reviewed. The double-blind peer-review was conducted on the basis of the full paper.
https://doi.org/10.5194/isprs-annals-XI-3-2026-307-2026 | © Author(s) 2026. CC BY 4.0 License.

2. Methodology

2.1 The Architecture of The Proposed Method

The overall architecture of the proposed LAD-Enhancer is illustrated in Figure 1. The network is trained in three sequential stages, where the parameters of each preceding stage are frozen during the training of subsequent stages. In the first stage, a lightweight convolutional linear layer performs binary classification to distinguish between clear and degraded images. In the second stage, the Mixture of Experts (MoE) restoration module processes the degraded images to recover structural and color information. Finally, in the third stage, the enhance module further refines the restored images to improve visual quality and detection performance. The parameter counts for the three stages are 273, 2406, and 251, respectively.

Since directly feeding clear images into the restoration module may lead to loss of original information, the initial classifier in the first stage is designed to identify whether the input image is degraded. Only degraded images are fed into the subsequent MoE restoration module. The classifier consists of a convolutional layer, normalization layer, pooling layer, and a fully connected layer, and its operation can be expressed as follows:

$$F_{\mathrm{m}} = f_{relu}\left(f_{BN}\left(f_{Conv1}\left(I_{Input}\right)\right)\right) \tag{1}$$

$$P_{IC} = f_{fc2}\left(f_{relu}\left(f_{fc1}\left(f_{Pooling}\left(F_m\right)\right)\right)\right) \tag{2}$$

where I_{Input} is the input of images, $f_{Conv1}(.)$ represents the 3 × 3 convolution layer, $f_{BN}(.)$ represents the batch normalization layer, $f_{relu}(.)$ denotes the ReLU activation function, $f_{Pooling}(.)$ is the pooling layer, $f_{fc1}(.)$ and $f_{fc2}(.)$ represent the fully connected layer. F_m and P_{IC} represent middle feature and the initial classification result probability, respectively. In this work, the P_{IC} threshold is set at 0.5.

After classification, clear images are directly forwarded to the downstream detection model, while degraded images are sent to the MoE restoration module for degradation-specific restoration. The second stage primarily focuses on training this module to enable the model to recognize and process different types of degradation, restoring each type accordingly.

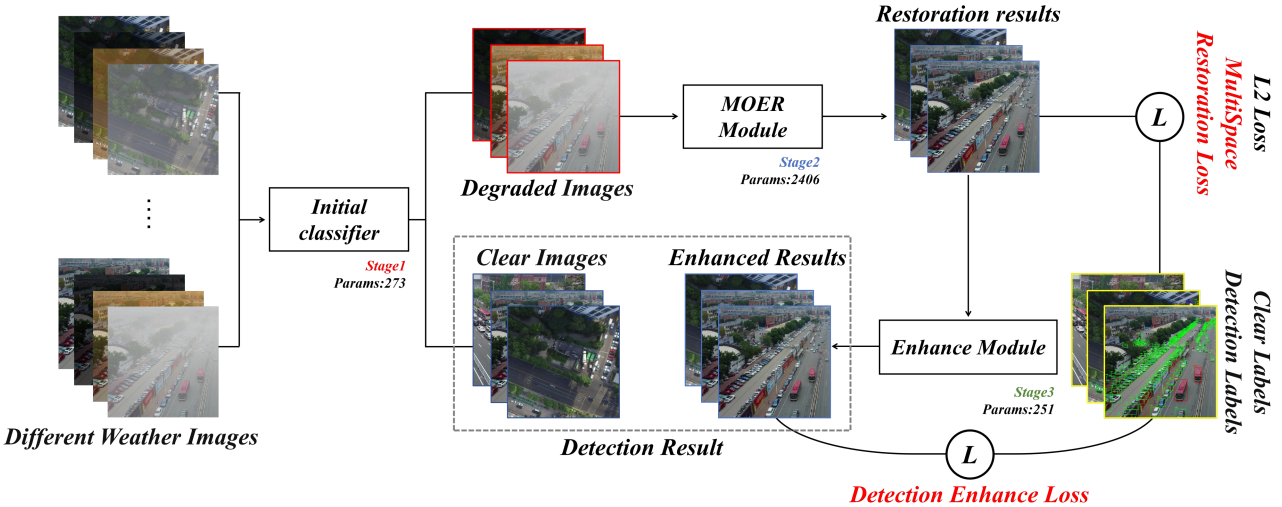

Figure 1. The Overall Framework of LAD-Enhancer.

In the third stage, the restored images are passed through the enhance module, which is trained using detection labels to strengthen the model’s perception of targets and improve the overall contrast of the enhanced results. The enhance module can be represented by the following process:

$$I_E = f_{Conv3}\left(f_{relu}\left(f_{Conv2}\left(I_R\right)\right)\right) \tag{3}$$

where I_E and I_R represent the enhanced images and the restoration images, respectively. Through its lightweight architecture and detection-enhanced loss, the enhance module effectively strengthens the model’s target perception capability.

Finally, both the enhanced results and the original clear images are input into the subsequent detection model. It is worth noting that the LAD-Enhancer outputs two results: the restored image and the enhanced image, allowing flexibility to support different downstream tasks.

2.2 Mixture of Experts Restoration Module

Although training the model with all degraded conditions simultaneously can provide it with certain general restoration capabilities, the differences among various degradation scenarios are substantial. Under the condition of a small number of model parameters, it is difficult for a single model to handle diverse restoration tasks across different conditions effectively. To address this challenge, we construct a Mixture of Experts (MoE) restoration module, which enables the model to distinguish between different types of degradation and process them separately. The overall structure of this module is illustrated in Figure 2.

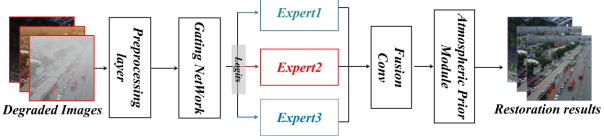

Figure 2. The structure of the Mixture of Experts Restoration Module.

Firstly, the degraded images are initially fed into the preprocessing layer to extract preliminary features. This process can be represented as:

$$F_P = f_{relu}\left(f_{Conv5}\left(f_{relu}\left(f_{Conv4}\left(I_D\right)\right)\right)\right) \tag{4}$$

where I_D and F_P represent the degraded images and the preprocessing features, respectively. Subsequently, the features extracted are fed into the gating network to obtain the

This contribution has been peer-reviewed. The double-blind peer-review was conducted on the basis of the full paper.
https://doi.org/10.5194/isprs-annals-XI-3-2026-307-2026 | © Author(s) 2026. CC BY 4.0 License.

probability representation of degradation classification. This process can be represented as:

$$V_P = f_{softmax}\left(f_{fc3}\left(f_{flatten}\left(f_{Pooling}\left(F_P\right)\right)\right)\right) \tag{5}$$

where $f_{softmax}(.)$ represents the softmax activation. $f_{softmax}(.)$ represents the the flattening operation. V_P represents the probability representation. Each expert process can subsequently be represented as:

$$F_E^i = f_{Cat}\left(f_{Conv6}\left(f_{relu}\left(F_P\right)\right), f_{Conv7}\left(f_{relu}\left(F_P\right)\right), f_{Conv8}\left(f_{relu}\left(F_P\right)\right)\right) \tag{6}$$

where $f_{Conv6}(.)$, $f_{Conv7}(.)$, $f_{Conv8}(.)$ denote multi-scale convolutions with kernel sizes 1 × 1, 3 × 3, and 5 × 5, respectively. $F_E^{\ i}$ denote the output of the i -th export. The expert restores the details and global features in the image more effectively through multi-scale fusion. During both the training and inference phases of the network, all three experts are activated, i.e., Top-3. The model inputs F_P into each of the three experts and then performs a weighted summation based on V_P. The fusion convolution process can be represented as:

$$F_{fusion} = f_{Conv9}\left(\sum_{i=1}^{i} F_E^{\ i} \cdot V_P^i\right) \tag{7}$$

The fusion features F_{fusion} are input into the Atmospheric Prior Module, where the atmospheric transfer equation is employed to enhance the robustness of the model. The process can be denoted as:

$$I_R = f_{relu}\left(F_{fusion} \cdot I_D - F_{fusion} + b\right) \tag{8}$$

where, b is a bias term set to 1 in this work. I_R are then fed into the enhancement module to obtain the enhanced results.

2.3 Multi-Stage Progressive Loss

To effectively guide model optimization at each stage, a multi-stage progressive loss function is designed. The model is trained in three independent stages, with the parameters of the preceding stage frozen during the training of each subsequent stage. Dedicated loss functions are developed for each stage according to their respective optimization objectives, ensuring effective and targeted model training.

Classification Loss Function: In the first stage, the initial classifier is trained, with the loss function being the Cross-Entropy Loss, which is formulated as follows:

$$\mathrm{L}_{IC} = \frac{1}{N}\sum_{i=1}^{N}\left[-y_i \cdot \log\left(\sigma\left(\hat{y}_i\right)\right) - \left(1-y_i\right) \cdot \log\left(1-\sigma\left(\hat{y}_i\right)\right)\right] \tag{9}$$

where y_i is the i -th true label, $\hat{y}_i$ is the i -th predicted results. The parameters of the first stage are trained via L_{IC} to enable the model to distinguish between clear and degraded images.

Detection Oriented Multi Space Restoration Loss Function: In the second stage, the loss function consists of two components. The first is the cross-entropy loss, which enables the model to distinguish between different types of degraded images. The second is the restoration loss, where the reconstructed images are compared with the corresponding clear labels to compute the supervised loss. Since color distortion can adversely affect target detection accuracy, the traditional RGB-channel L2 loss is complemented with losses in the HSV and LAB color spaces, forming a multi-space restoration loss. This loss can be expressed as:

$$\mathrm{L}_{RGB} = f_{L_2}\left(I_R, I_C\right) \tag{10}$$

$$\mathrm{L}_{HSV} = f_{L_2}\left(f_{HSV}\left(I_R\right), f_{HSV}\left(I_C\right)\right) \tag{11}$$

$$\mathrm{L}_{LAB} = f_{L_2}\left(f_{LAB}\left(I_R\right), f_{LAB}\left(I_C\right)\right) \tag{12}$$

$$\mathrm{L}_{MSR} = L_{RGB} + L_{HSV} + L_{LAB} \tag{13}$$

where $f_{L2}(.)$, $f_{HSV}(.)$, $f_{LAB}(.)$ represent the L2 loss, the RGB to HSV transformation, and the RGB to LAB transformation, respectively. Different color space channels exhibit varying degrees of sensitivity to color differences, as shown in Figure 3. By employing a multi space restoration loss, the color differences can be comprehensively restored.

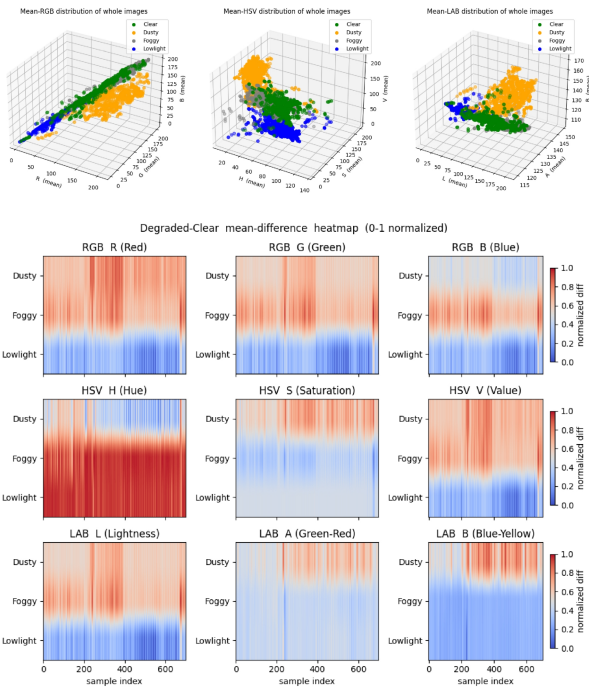

Figure 3. Visualization of multi-space channel scatter plots under various degraded weather conditions.

Detection Enhance Loss Function: In the third stage, the detection enhance loss is calculated using the detection labels to focus the model's attention on the targets and enhance the contrast of the results. This loss can be expressed by the following formula:

$$\mathrm{L}_{DE} = f_{L_2}\left(f_{Mask}\left(I_R\right), f_{Mask}\left(I_C\right)\right) \tag{14}$$

This contribution has been peer-reviewed. The double-blind peer-review was conducted on the basis of the full paper.
https://doi.org/10.5194/isprs-annals-XI-3-2026-307-2026

where L_{DE} represents the detection enhance loss, $f_{Mask}(.)$ represent the mask operation, only calculating the object part loss.

3. Experiment

In the experimental section, the proposed LAD-Enhancer is comprehensively evaluated for its ability to restore and detect images under various degraded and clear conditions for the detection model.

3.1 Implementation Details

All experiments were conducted using an NVIDIA GeForce GTX 4080 GPU with 16GB RAM. The detection model employs DiffusionDet(Chen et al., 2022) trained by clear images as the baseline, and the detector parameters remain unchanged throughout the experimental process. During the first stage of training, the enhancer, the batch size is set to 12, with half of the images being clear and the other half being degraded. Subsequently, in the second stage of training, the mixture of experts’ models, the batch size is set to 16, with four images randomly selected under each condition (foggy, dusty, low-light, and clear) to prevent the model from experiencing catastrophic forgetting during training. During training, the initial learning rate is set to 2^{-3}, and the final learning rate is set to 2^{-5}. The optimizer used is Adam (Loshchilov and Hutter, 2017).

Figure 4. The Multi-Degradation Aerial Detection Dataset.

The dataset used in this study was developed in a prior unpublished work and includes simulated degraded aerial images under foggy, dusty, and low-light conditions, as shown in Figure 4. It also contains a real-world aerial detection test set collected under adverse weather conditions, which was used for evaluation in this paper.

To comprehensively assess performance, four groups of experiments were conducted: (1) model restoration performance comparison, (2) model detection performance comparison, (3) model component and loss ablation studies, and (4) overall model performance comparison.

The comparison methods included deep learning-based dehazing algorithms: AODNet(Li et al., 2017), GirdDehazeNet(Liu et al., 2019), FFANet(Qin et al., 2020), MB-TalyorFormer(Qiu et al., 2023), and the all-in-one restoration models IDR(Zhang et al., 2023), MOCE-IR(Zamfir et al., 2024). For detection performance evaluation, the restored images were directly fed into a detector pretrained on clear images to assess plug-and-play compatibility and performance improvement before integration into the detection pipeline. To ensure fairness, all comparison models were trained using the same dataset, which included both degraded and clear images.

3.2 Restoration Performance Comparison Experiment

In this experiment, PSNR, SSIM, RMSE, and SAM were selected as evaluation metrics to assess restoration performance. All comparison methods are image restoration models, which contain significantly more parameters than the proposed LAD-Enhancer. The quantitative results are presented in Table 1, where the best performances are highlighted in bold and the integrated approach is denoted with an asterisk *. Overall, the proposed LAD-Enhancer exhibits slightly lower restoration accuracy than the all-in-one restoration models but achieves comparable performance with a fraction of their parameter count. Furthermore, it outperforms models that lack all-in-one processing capability. The visual restoration results are shown in Figure 5.

From the visualization, models trained on multiple types of degraded data but a non-all-in-one restoration strategy fail to generalize effectively across diverse degradation scenarios. In contrast, the proposed LAD-Enhancer produces results visually similar to those of the all-in-one restoration models, demonstrating strong adaptability.

Additionally, Figure 6 presents the restoration results of the proposed enhancer on aerial images captured under real adverse weather conditions. The results indicate that the proposed LAD-Enhancer effectively restores overall image clarity and structure, confirming its practical applicability in real-world aerial imaging scenarios.

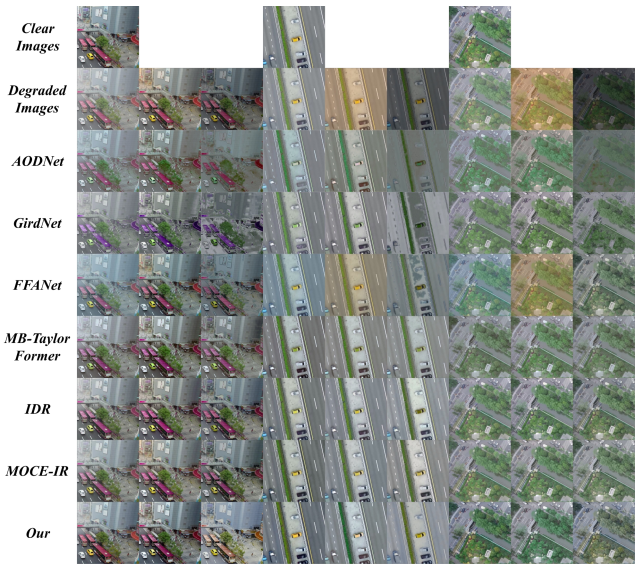

Figure 5. Restoration Visualization Results.

Figure 6. Restoration Visualization Results in real-world scenario.

This contribution has been peer-reviewed. The double-blind peer-review was conducted on the basis of the full paper.
https://doi.org/10.5194/isprs-annals-XI-3-2026-307-2026 | © Author(s) 2026. CC BY 4.0 License.

Table 1. Restoration Performance Comparison Result.

	Foggy Condition				Dusty Condition				Lowlight Condition			
	PSNR	SSIM	RMSE	SAM	PSNR	SSIM	RMSE	SAM	PSNR	SSIM	RMSE	SAM
AODNet	28.806	0.7735	9.370	0.2247	28.789	0.8512	9.328	0.1691	27.968	0.6648	10.198	0.2793
GirdNet	28.993	0.7830	9.167	0.2114	30.282	0.8824	7.920	0.1207	28.538	0.7529	9.590	0.2483
FFANet	28.470	0.8016	9.695	0.2068	28.927	0.8729	9.212	0.1885	28.662	0.8068	9.505	0.1590
TalyorFormer	29.255	0.8345	8.957	0.1624	30.141	0.8997	8.061	0.1104	28.720	0.8274	9.431	0.1412
IDR*	**29.705**	0.8444	**8.545**	0.1477	**31.384**	0.9089	**6.993**	**0.0888**	29.150	0.8540	8.965	**0.1221**
MOCE-IR*	29.602	**0.8455**	8.646	**0.1465**	31.180	**0.9091**	7.172	0.1026	**29.194**	**0.8544**	**8.924**	0.1269
Our*	28.777	0.8361	9.367	0.1587	30.708	0.9010	7.535	0.1037	28.500	0.8148	9.637	0.1430

3.3 Detection Performance Comparison Experiment

In the detection performance comparison experiment, the restoration results of each model were directly fed into the baseline detector trained on clear images. Using a plug-and-play approach, we compared the improvements in detection performance achieved by the restoration and enhancement results of each model. The detection accuracy was evaluated using the mAP50 metric. The experimental results are presented in Table 2. The first to fourth columns represent the detection performance of the model on datasets under adverse weather conditions, while the fifth column represents the detection performance under real-world adverse weather conditions.

Table 2. Detection Performance Comparison Result.

	Clear	Foggy	Dusty	Low light	Real
Baseline	65.853	50.971	48.038	57.494	24.247
AODNet	61.312	48.864	55.016	40.108	20.875
GirdNet	60.259	49.545	58.820	48.250	20.622
FFANet	64.675	50.368	53.296	58.970	24.100
Taylor Former	62.735	53.219	61.477	58.733	25.221
IDR*	64.892	54.435	61.550	58.530	25.545
MOCE -IR*	64.238	54.030	61.141	**59.141**	25.561
Our*	**65.379**	**55.290**	**61.879**	58.985	**26.668**

Experimental results show that LAD-Enhancer, with only minimal additional parameters, comprehensively improves the detection performance of the original baseline in adverse weather conditions while maintaining nearly unchanged detection performance on clear images.

Although the proposed LAD-Enhancer does not surpass some methods in terms of restoration metrics, it achieves the best performance on four of the five test sets in the detection task and is second only to the baseline detector on the low-light dataset. The detection visualization results are shown in Figures 7 and 8. These visualizations demonstrate that LAD-Enhancer, with minimal parameters and negligible inference speed overhead, significantly improves the performance of the baseline detector in both simulated and real-world scenarios.

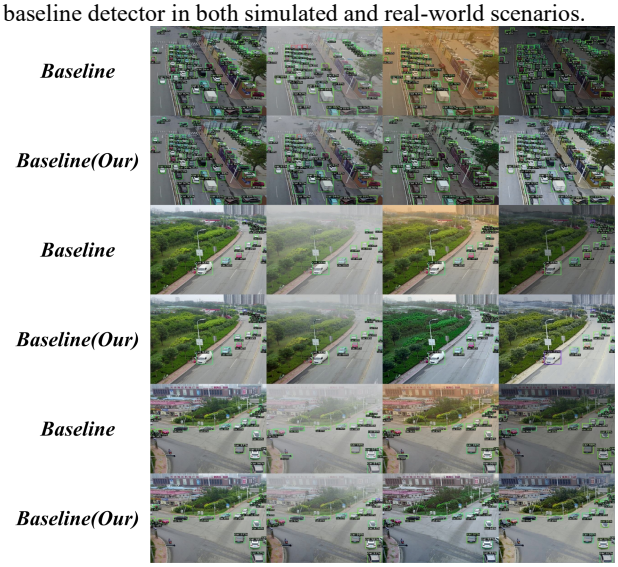

Figure 7. Detection Visualization Result in simulated scenarios.

Figure 8. Detection Visualization Result in real scenarios.

The radar visualization of the experimental results is shown in Figure 9. With an increase of only 2,930 parameters, the total performance of the detection evaluation metric mAP50 was improved by 21.598 across five test sets, including the test set with real complex data.

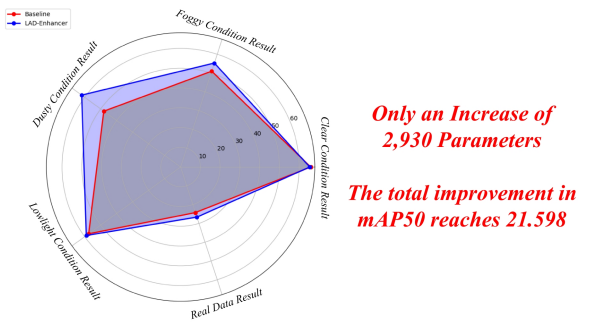

Figure 9. The radar visualization of the experimental results.

https://doi.org/10.5194/isprs-annals-XI-3-2026-307-2026

3.4 Component Ablation Experiment

In the component ablation experiments, ablations were conducted on the basic Mixture of Experts Restoration Module with L2, the Multi Space Restoration Loss, the initial classifier, and enhance module with the detection enhancement loss. The experimental results are presented in Table 3. The results of the ablation experiments show that optimizing the Mixture of Experts Restoration Module using only the L2 loss can enhance the original baseline's performance in foggy and dusty conditions. However, this approach leads to a decrease in performance under low-light conditions. The added Multi Space Restoration Loss effectively constrains the restoration results in low-light scenarios.

Furthermore, feeding the original clear images into the enhancer results in a significant drop in detection performance. The proposed initial classifier effectively addresses this issue. Finally, the enhancement mechanism focuses the restoration results on the targets and enhances the contrast of the results, thereby comprehensively improving the detector's performance under adverse weather conditions.

Table 3. Component Ablation Experiments Result.

	Clear	Foggy	Dusty	Low light	Real
Baseline	65.853	50.971	48.038	57.494	24.247
MOER Module	61.178	54.092	61.418	49.512	25.137
MSR Loss	61.125	54.139	61.569	57.258	25.922
Initial Classifie	65.454	53.931	61.268	57.932	26.015
Enhance	65.379	55.290	61.879	58.985	26.668

3.5 Comprehensive Performance Comparison Experiment

To comprehensively evaluate the performance of the proposed LAD-Enhancer, we compared it with the current best methods in terms of parameter count, inference speed, and detection accuracy on a real-world test set. The experimental results show that compared with well-performing comparison methods, the proposed method reduces the number of parameters by approximately 100 times while increasing the speed by more than 10 times, as shown in Table 4. This is particularly valuable for aerial detection tasks that require edge deployment and real-time inference. Furthermore, compared with other methods, the enhanced results of the proposed model also achieve the best detection performance. The comprehensive comparison results are then visualized in Figure 10. The visualization more clearly demonstrates the improvement in detection performance and the application value of the proposed model.

Table 4. Comprehensive Performance Comparison Result.

	Params(M)	Inference Speed(ms)	Real
AODNet	0.001761	0.0010	20.875
GirdNet	0.958051	0.0071	20.622
FFANet	4.455913	0.0148	24.100
TalyorFormer	2.676520	0.0775	25.221
IDR	2.985088	0.0234	25.545
MOCE-IR	2.950402	0.0265	25.561
Our	0.002930	0.0020	26.668

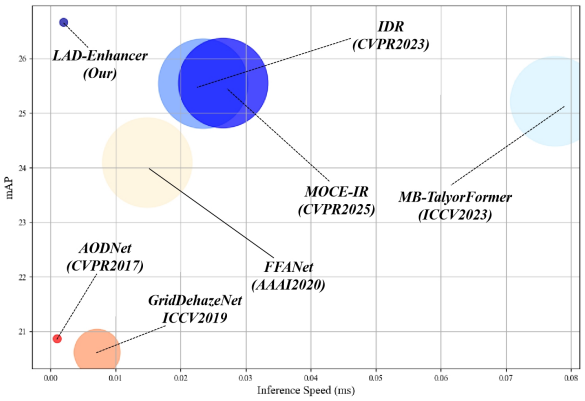

Figure 10. Visualization of Comprehensive Performance.

4. Conclusion

In this paper, we propose an LAD-Enhancer for detection tasks, which can be plugged into the detector to enhance its performance under adverse weather conditions without the need to adjust the detector's parameters. Meanwhile, in response to the complex detection environment of aerial detection tasks, we designed an Initial Classifier and a Mixture of Experts Restoration Module, enabling the model to accurately identify different weather conditions and perform condition-specific restoration. Furthermore, we construct a Multi-Stage Progressive Loss to effectively constrain each stage. In this constraint criterion, to mitigate the effects of color distortion and contrast reduction commonly observed in degraded images, we propose a Multi-Space Restoration Loss and an enhancement module with detection-oriented loss functions. These designs effectively improve detection robustness and accuracy under various degradation scenarios. In future work, we plan to deploy the proposed model on aerial platforms such as drones to evaluate its real-time performance in practical applications.

References

Badgujar, C.M., Poulose, A. and Gan, H., 2024. Agricultural object detection with You Only Look Once (YOLO) Algorithm: A bibliometric and systematic literature review. Computers and Electronics in Agriculture, 223: 18.

Chen, S., Sun, P., Song, Y. and Luo, P., 2022. DiffusionDet: Diffusion Model for Object Detection. 2023 IEEE/CVF International Conference on Computer Vision (ICCV): 19773-19786.

Huang, S.C., Le, T.H. and Jaw, D.W., 2021. DSNet: Joint Semantic Learning for Object Detection in Inclement Weather Conditions. Ieee Transactions on Pattern Analysis and Machine Intelligence, 43(8): 2623-2633.

Li, B.Y., Peng, X.L., Wang, Z.Y., Xu, J.Z., Feng, D. and Ieee, 2017. AOD-Net: All-in-One Dehazing Network, 16th IEEE International Conference on Computer Vision (ICCV). IEEE International Conference on Computer Vision. Ieee, Venice, ITALY, pp. 4780-4788.

Li, Y. and Zhao, Y.F., 2023. RSID: A Remote Sensing Image Dehazing Network, 6th Chinese Conference on Pattern Recognition and Computer Vision (PRCV). Lecture Notes in Computer Science. Springer-Verlag Singapore Pte Ltd, Xiamen Univ, Xiamen, PEOPLES R CHINA, pp. 3-14.

Liu, X.H., Ma, Y.R., Shi, Z.H., Chen, J. and Ieee, 2019. GridDehazeNet: Attention-Based Multi-Scale Network for Image Dehazing, IEEE/CVF International Conference on

Computer Vision (ICCV). IEEE International Conference on Computer Vision. Ieee, Seoul, SOUTH KOREA, pp. 7313-7322.

Long, J., Shi, Z.W., Tang, W. and Zhang, C.S., 2014. Single Remote Sensing Image Dehazing. Ieee Geoscience and Remote Sensing Letters, 11(1): 59-63.

Loshchilov, I. and Hutter, F., 2017. Decoupled Weight Decay Regularization, pp. arXiv:1711.05101.

Qin, X., Wang, Z.L., Bai, Y.C., Xie, X.D., Jia, H.Z. and Assoc Advancement Artificial, I., 2020. FFA-Net: Feature Fusion Attention Network for Single Image Dehazing, 34th AAAI Conference on Artificial Intelligence / 32nd Innovative Applications of Artificial Intelligence Conference / 10th AAAI Symposium on Educational Advances in Artificial Intelligence. AAAI Conference on Artificial Intelligence. Assoc Advancement Artificial Intelligence, New York, NY, pp. 11908-11915.

Qiu, Y.W., Zhang, K.H., Wang, C.X., Luo, W.H., Li, H.D., Jin, Z. and Ieee, 2023. MB-TaylorFormer: Multi-branch Efficient Transformer Expanded by Taylor Formula for Image Dehazing, IEEE/CVF International Conference on Computer Vision (ICCV). IEEE International Conference on Computer Vision. Ieee Computer Soc, Paris, FRANCE, pp. 12756-12767.

Wan, Y., Li, J., Lin, L., Yuan, Q. and Shen, H., 2025. Collaboration of Dehazing and Object Detection Tasks: A Multi-Task Learning Framework for Foggy Image. IEEE Transactions on Geoscience and Remote Sensing: 1-1.

Wang, C., Li, C., Luo, B., Wang, W. and Liu, J., 2021. RiWNet: A moving object instance segmentation Network being Robust in adverse Weather conditions, pp. arXiv:2109.01820.

Xia, J., Chen, T. and Qiao, J., 2022. Vehicle Detection Based on YOLOv3 in Adverse Weather Conditions, 2022 IEEE 4th International Conference on Civil Aviation Safety and Information Technology (ICCASIT), pp. 692-696.

Yang, S., Lu, H.M. and Li, J.R., 2023. Multifeature Fusion-Based Object Detection for Intelligent Transportation Systems. Ieee Transactions on Intelligent Transportation Systems, 24(1): 1126-1133.

Zamfir, E., Wu, Z., Mehta, N., Tan, Y., Paudel, D.P., Zhang, Y. and Timofte, R., 2024. Complexity Experts are Task-Discriminative Learners for Any Image Restoration. 2025 IEEE/CVF Conference on Computer Vision and Pattern Recognition (CVPR): 12753-12763.

Zhang, J.H., Huang, J., Yao, M.D., Yang, Z.Z., Yu, H., Zhou, M., Zhao, F. and Ieee, 2023. Ingredient-oriented Multi-Degradation Learning for Image Restoration, IEEE/CVF Conference on Computer Vision and Pattern Recognition (CVPR). IEEE Conference on Computer Vision and Pattern Recognition. Ieee Computer Soc, Vancouver, CANADA, pp. 5825-5835.

Zhang, Y., Xue, J.R., Zhang, G., Zhang, Y.W., Zheng, N.N. and Ieee, 2014. A Multi-Feature Fusion Based Traffic Light Recognition Algorithm for Intelligent Vehicles, 33rd Chinese Control Conference (CCC). Chinese Control Conference. Ieee, Nanjing, PEOPLES R CHINA, pp. 4924-4929.

Zhang, Z., Yan, J., Liang, Y., Feng, J., He, H. and Cao, L., 2025. Multiscale Restoration of Missing Data in Optical Time-Series Images With Masked Spatial–Temporal Attention Network. IEEE Transactions on Geoscience and Remote Sensing, 63: 1-15.

Zhang, Z., Zhao, L., Liu, Y., Zhang, S. and Yang, J., 2020. Unified Density-Aware Image Dehazing and Object Detection in Real-World Hazy Scenes, Asian Conference on Computer Vision.

Zhao, C.J., Liu, R.W., Qu, J.X. and Gao, R.B., 2024. Deep learning-based object detection in maritime unmanned aerial vehicle imagery: Review and experimental comparisons. Engineering Applications of Artificial Intelligence, 128: 21.